Rotation of the magnetic vortex lattice in Ru_7B_3 driven by the effects of broken time-reversal and inversion symmetry

A. S. Cameron,[1] Y. S. Yerin,[1,2] Y. V. Tymoshenko,[1] P. Y. Portnichenko,[1] A. S. Sukhanov,[3,1] M. Ciomaga Hatnean,[4] D. Mc K. Paul,[4] G. Balakrishnan,[4] R. Cubitt,[5] A. Heinemann,[6] and D. S. Inosov[1]

[1]*Institut für Festkörper- und Materialphysik, Technische Universität Dresden, D-01069 Dresden, Germany*

[2]*Physics Division, School of Science and Technology, Università di Camerino, Via Madonna delle Carceri 9, I-62032 Camerino (MC), Italy*

[3]*Max Planck Institute for Chemical Physics of Solids, D-01187 Dresden, Germany*

[4]*Department of Physics, University of Warwick, Coventry, CV4 7AL, United Kingdom*

[5]*Institut Laue-Langevin, 71 avenue des Martyrs, CS 20156, F-38042 Grenoble Cedex 9, France*

[6]*German Engineering Materials Science Centre (GEMS) at Heinz Maier-Leibnitz Zentrum (MLZ), Helmholtz-Zentrum Geesthacht GmbH, D-85748 Garching, Germany*

(Received 9 October 2018; revised manuscript received 15 April 2019; published 26 July 2019)

We observe a hysteretic reorientation of the magnetic vortex lattice in the noncentrosymmetric superconductor Ru_7B_3, with the change in orientation driven by altering the magnetic field below T_c. Normally a vortex lattice chooses either a single or degenerate set of orientations with respect to a crystal lattice at any given field or temperature, a behavior well described by prevailing phenomenological and microscopic theories. Here, in the absence of any typical VL structural transition, we observe a continuous rotation of the vortex lattice which exhibits a pronounced hysteresis and is driven by a change in magnetic field. We propose that this rotation is related to the spontaneous magnetic fields present in the superconducting phase, which are evidenced by the observation of time-reversal symmetry breaking, and the physics of broken inversion symmetry. Finally, we develop a model from the Ginzburg-Landau approach which shows that the coupling of these to the vortex lattice orientation can result in the rotation we observe.

DOI: 10.1103/PhysRevB.100.024518

I. INTRODUCTION

Interest in noncentrosymmetric (NCS) superconductors has greatly increased since the discovery of the heavy-fermion superconductor $CePt_3Si$ [1], and novel superconducting states with unusual properties have been predicted. The key physics in NCS superconductors is that of antisymmetric spin-orbit coupling (ASOC), which spin-splits the Fermi surface, removes the conservation of parity, and permits the mixing of *s*- and *p*-wave states [2–5]. Singlet-triplet mixing has only been observed in some cases, as both must be allowed by the pairing mechanism, and the ASOC must be strong enough for the effects to become noticeable. Perhaps the best known example is the case of $Li_2Pd_3B_3$ and $Li_2Pt_3B_3$, where the Pd system appeared to have a predominantly spin-singlet order parameter while the larger spin-orbit coupling in the Pt system resulted in a dominant triplet component, and thus line nodes in the energy gap as evidenced by penetration depth measurements [6].

An order parameter consisting of a singlet-triplet mixture should strongly affect the electronic states around a vortex core [7,8], and can potentially introduce nodes in the gap not demanded by symmetry [9,10]. Vortex core anisotropies and nodal gaps are well known to result in structural phase transitions of the vortex lattice (VL) as the applied magnetic field and temperature are varied [11,12], and as such the VL may be an ideal probe to investigate broken inversion symmetry. Thus, VL structure transitions are not unusual, having been observed in classical superconductors [11], cuprates [13–16], pnictides [17,18], and others [19], to name but a few. In theory, these transitions are generally described as resulting from anisotropy in either the superconducting gap [20], Fermi velocity [21–23], or both [12,24] and are driven by thermal fluctuations at a transition line in the manner of a classical phase transition. VL structures which show a gradual field and temperature dependence are also known, which can be driven by the same physics as the structural transitions described above, but also by multigap physics in the case of MgB_2, where the VL undergoes a smooth rotation as a function of field [25,26]. While to date the theories focusing on gap and Fermi velocity anisotropy have not been adapted for NCS superconductors, the effect of broken inversion symmetry on the VL has been the subject of multiple studies [8,27–30], which have focused on the C_{4v} and O crystallographic point groups. Perhaps the most striking result from these investigations has been the appearance of a transverse component of magnetic field in the vortex lattice [9,27,28,31–33], which arises due to currents flowing parallel to the vortex which are unique to NCS systems. Further, the emergence of a new gap-amplitude modulated phase has been predicted in superconductors with nonzero Rashba-type spin-orbit coupling, which should have a strong effect on the VL coordination [29,30], although to date neither of these has been directly observed. To our knowledge, the only NCS superconductor where the VL morphology has been studied is BiPd [34], which displayed an intermediate mixed state but otherwise showed no signs of unconventional behavior related to broken inversion symmetry.

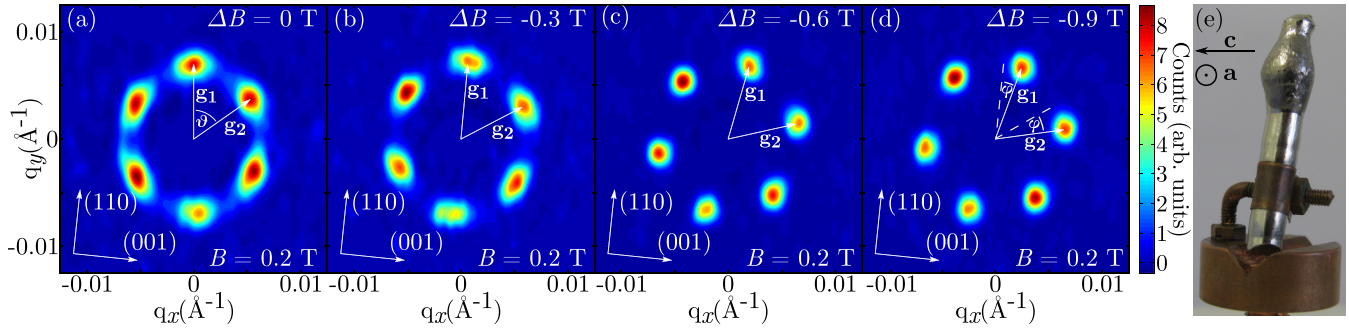

FIG. 1. Diffraction patterns from the VL taken at 0.2 T along the **a** axis after different field histories: (a) $0 \rightarrow 0.2$ T, (b) $0 \rightarrow 0.5 \rightarrow 0.2$ T, (c) $0 \rightarrow 0.9 \rightarrow 0.2$ T, and (d) $0 \rightarrow 1.1 \rightarrow 0.2$ T. The magnitude of the decrease in magnetic field prior to measurement is indicated as ΔB. The reciprocal space lattice vectors of the VL, $\mathbf{g_1}$ and $\mathbf{g_2}$, are shown for each diffraction pattern. The angle between the two basis vectors, θ, is shown in panel (a), while the orientation of the lattice with respect to the FC lattice, ϕ, is shown in panel (d). (e) Photograph of the sample, with the orientation of the **a** and **c** axes indicated.

Here we employ small-angle neutron scattering (SANS) to study the VL in another NCS superconductor, Ru_7B_3. It forms a NCS crystal structure with the space group $P6_3mc$ [35], which is hexagonal in the basal plane. Our single-crystal sample has a superconducting transition temperature of $T_c = 2.6$ K [36], which sits within the range of 2.5 to 3.4 K observed in earlier studies [37–39]. It is reported to have an isotropic *s*-wave gap [38], rather than the singlet-triplet mixture predicted for NCS superconductors. Specific-heat and magnetization measurements on a single crystal of Ru_7B_3 resulted in Ginzburg-Landau parameters of 21.6 and 25.5 for the [100] and [001] directions, respectively [39], making it a reasonably strong type-II superconductor.

II. EXPERIMENTAL DETAILS

SANS measurements were performed on the D33 instrument [40] at the Institut Laue-Langevin (ILL) in Grenoble, France [41,42], and the SANS-I instrument at the Heinz Maier-Leibnitz Zentrum (MLZ) in Garching, Germany [43]. Incoming neutrons were velocity selected with a wavelength between 8 and 14 Å, depending on the measurement, with a full width at half maximum (FWHM) spread in wavelength of ∼10%, and diffracted neutrons were measured using a position-sensitive detector. The sample, shown in Fig. 1(e), is roughly cylindrical with a diameter of ∼5 mm and a length of ∼30 mm. It was mounted on a copper holder with the **a** and **c** directions in the horizontal plane and placed in a dilution refrigerator (ILL) or a ^{3}He cooler (MLZ) within a horizontal-field cryomagnet with the magnetic field applied along the neutron beam. For measurements with the dilution refrigerator, the sample was cooled in no applied field (zero field cooled, or ZFC), as the T_c of the sample was above the maximum stable temperature of the system, and the magnetic field was applied and changed while at base temperature, which was either 55 mK or 1.1 K. When using the ^{3}He cooler, the sample could be cooled in field (field cooled, or FC) as the system was stable above T_c, and measurements were taken at a base temperature of 0.5 K. Measurements, such as those in Fig. 1, were taken by holding the applied field and temperature constant and rocking the sample throughout all the angles that fulfill the Bragg conditions for the first-order diffraction spots of the VL. Background measurements were taken in zero field and then subtracted from the in-field measurements to leave only the VL signal. Diffraction patterns were treated with a Bayesian method for handling small-angle diffraction data, detailed in Ref. [44].

III. RESULTS

Now we turn to the presentation of SANS data on Ru_7B_3. We focus on measurements at 0.2 T and above, as below this field the strength of the vortex pinning is high enough to disorder the VL, which complicates diffraction measurements. For magnetic fields applied along the **a** axis we observe a hexagonal VL with a small degree of anisotropy, on the order of 9%, up to the maximum measured field of 1 T. However, we find that the orientation of the VL with respect to the crystal lattice is not simply dependent on the magnitude of the applied field, as it is common in many superconductors, but on the field history when below the critical temperature. Figure 1 shows diffraction patterns all taken at 0.2 T, and we observe the orientation of the VL change significantly depending on the field history of the sample. Panel (a) shows the VL at 0.2 T, applied from zero field at 55 mK. In this diffraction pattern, we find that the reciprocal space lattice vector $\mathbf{g_1}$ lies at $\sim -6^\circ$ from the (110) crystal lattice direction. However, when the VL is prepared through the FC procedure, we find $\mathbf{g}_1 \parallel (110)$, and so therefore we define the field-cooled lattice as the equilibrium orientation and will measure other orientations with respect to this. We will define the angle between the basis vectors of the FC lattice and the basis vectors of an arbitrary lattice as the orientation, denoted ϕ in Fig. 1(d). Panels (b)–(d) show the VL at 0.2 T, but prepared after a decrease in magnetic field following the ZFC procedure, while held at 55 mK. The VL undergoes a clockwise rotation as the field is decreased, with a change in field of −0.9 T rotating the VL by around 25°. We refer to this as a rotation of the VL, although we must point out that SANS is unable to distinguish a local reorientation of vortex nearest neighbors from a bulk rotation of the VL as a whole.

Figure 2 presents a numerical representation of the rotation of the VL for magnetic field applied parallel to the **a** axis. Panel (a) shows the rotation of the VL as a function of the

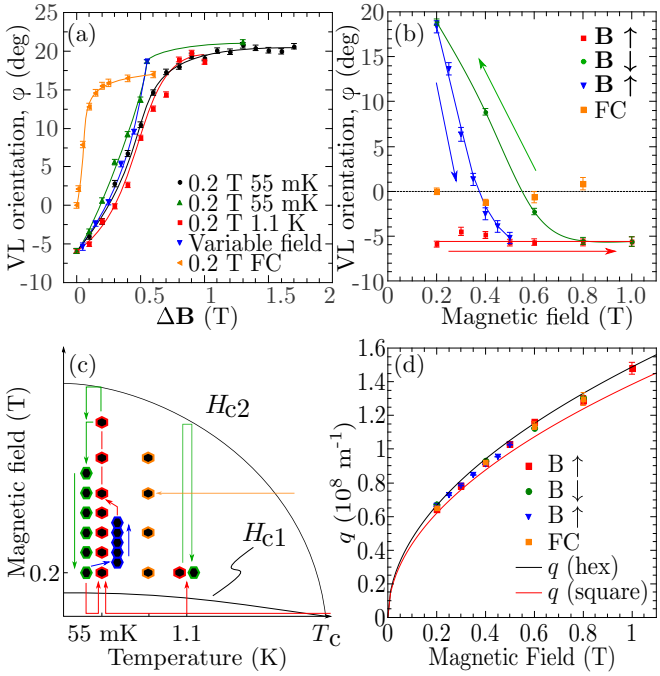

FIG. 2. (a) Orientation of the VL, ϕ, as a function of the change in magnetic field prior to measurement. (b) Orientation of the VL, ϕ, as a function of absolute magnetic field at 55 mK. Lines are guides for the eyes. (c) Schematic phase diagram indicating the data presented in this paper and the field/temperature paths used to obtain them, where the H_{c1} and H_{c2} lines are guides for the eye. Four separate sets of hexagons are shown, indicating the ZFC lattice (red), FC lattice (orange), rotated by decreasing field (green), and rotated by increasing field (blue) VL orientations. (d) The magnitude of the scattering vector, q, for the first-order Bragg reflections as a function of field, corresponding to the data of panel (b).

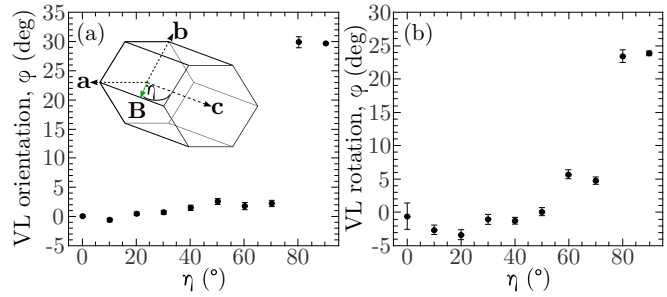

FIG. 3. (a) The orientation of the VL as a function of the angle, η, between the applied magnetic field and the **c** axis of the crystal. The VL orientation was measured with respect to the equilibrium state VL in the basal plane (**B** ∥ **c**). The inset illustrates a unit cell of the crystal and the orientation of the magnetic field. (b) Rotation of the VL, after a −0.8 T change in applied magnetic field, as a function of the angle between the magnetic field and the basal plane of the crystal. The orientation of the VL was measured with respect to the 0.2 T ZFC lattice at the same angle between the field and basal plane. All measurements were taken at 0.2 T and 55 mK.

decrease in magnetic field prior to measurement. The lattice was prepared by the ZFC method for all measurements except for the single data set labeled "0.2 T FC", and then the applied field was decreased by the amount indicated on the graph. Two of the data sets, taken during separate experiments, were both measured at 0.2 T and 55 mK and correspond to the data in Fig. 1. They show the same behavior, although with a slight change in the rate of rotation which is probably due to a small difference in the alignment of the magnetic field with respect to the crystal axes, as all other experimental conditions were the same, and later data presented here indicate that the VL rotation is dependent on this alignment. These measurements were repeated at 1.1 K, which is $\sim 0.42\,T/T_c$, and show the same behavior, indicating that the rotation is temperature independent. In the measurement labeled "variable field", the diffraction patterns were taken at different fields, but the starting field before the decrease prior to measurement was kept the same: 0.75 T. The rotation of the VL after being prepared by the FC method at 0.5 K is shown in the final data set, and here we see that the lattice initially rotates at a faster rate than after having been prepared by the ZFC method.

Figure 2(b) plots the orientation of the VL as a function of magnetic field, with one set prepared by the FC method at all fields and the other taken sequentially after preparing a ZFC 0.2 T VL, while remaining at 55 mK. The FC VL is oriented roughly at $\phi = 0$ for all fields. The order of measurement of the sequential data is indicated by the arrows and follows the legend from the top down. As the magnetic field is increased from the 0.2 T ZFC lattice, the VL remains at roughly −6° up to the highest measured field of 1 T. Following this, the magnetic field is decreased and we see the lattice begin to rotate, reaching an angle of 25° after returning to 0.2 T. The magnetic field was then increased again, and the lattice was seen to rotate back in an anticlockwise direction much faster than the initial clockwise rotation, returning to its initial orientation at around 0.5 T. Therefore, it appears that changing magnetic field below T_c always induces a rotation of the VL; however this rotation has saturation points at around −6° and 20°.

Figure 2(c) presents a schematic phase diagram, showing the measurements presented in this paper for fields parallel to the **a** axis, and the paths taken in field and temperature used to prepare the VL. Four categories of VL are indicated: The FC orientation, the ZFC orientation, the lattice rotated by decreasing field, and the lattice rotated by increasing field. The legend follows the same color scheme as panel (b). The magnitude of the scattering vector, q, as a function of applied magnetic field is presented in Fig. 2(d), and corresponds to the data taken in panel (b). The predicted q for square and hexagonal lattices are shown by solid lines.

Figure 3 describes the orientation and rotation of the VL as a function of the angle η between the applied magnetic field and the **c** axis. Panel (a) plots the orientation of the ZFC VL at 0.2 T and 55 mK, measured with respect to the same conditions with the magnetic field applied parallel to the **c** axis. The inset shows an illustration of the unit cell defining the angle η between the magnetic field and the **c** axis. Panel (b) shows the rotation of the VL after a −0.8 T change in magnetic field, measured with respect to the 0.2 T ZFC lattice at the same angle of magnetic field, η. We see in panel (a) that between $\eta = 70°$ and $\eta = 75°$ there is a reorientation of the VL of around 30°, and that rotation of the VL as a function of changing field below T_c emerges across this reorientation as the angle η approaches 90° where the field is in the **ab** plane.

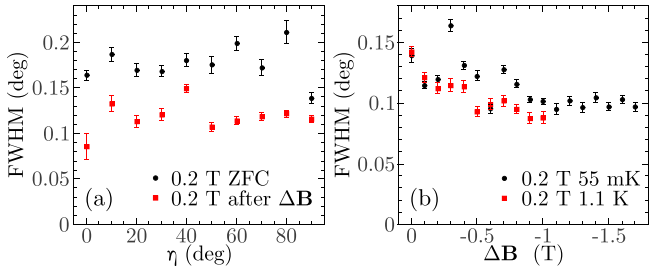

FIG. 4. (a) The FWHM of rocking curves at 0.2 T as a function of η, for the ZFC lattice and after a field change of -0.8 T. (b) The FWHM of rocking curves at 0.2 T as a function of change in field prior to the measurement, corresponding to the data from Fig. 2(a).

Figure 4 presents the FWHM of rocking curves when fitted to a Lorentzian line shape. Panel (a) presents data as a function of the angle η, corresponding to the data in Fig. 3, for both the ZFC lattice and data after a change in field of -0.8 T, all taken at 0.2 T. Panel (b) gives the FWHM for data taken at 0.2 T with the field in the plane, as a function of the change in field prior to the measurement. Data were taken at 55 mK and 1.1 K, and are from the corresponding scans in Fig. 2(a).

IV. DISCUSSION

The observed rotation is clearly very unusual, and to illustrate this we will briefly compare it to the VL structural transitions in centrosymmetric systems. As discussed in the introduction, it is both predicted in theory and found in experiment that changes in the VL morphology have single-valued behavior as the field and temperature are varied [12,20–24]. Furthermore, at least in the absence of strong vortex pinning, it is a general result that the VL structure is independent of the thermodynamic path taken to produce it, a conclusion supported by an experiment, for example, on NbSn, where the VL structure was found to be the same for both FC and ZFC preparations [45]. This is in stark contrast to the behavior we observe in Ru_7B_3, where at no point can a typical structural transition be defined, but rather it is the process of changing magnetic field which acts as the driving force of the rotation. This is illustrated explicitly in Fig. 2(a) when comparing the "0.2 T 55 mK" scans with the "variable field 55 mK" data, which show the same rotation of the VL for equal changes in magnetic field whose paths in terms of absolute magnetic field have no overlap. We therefore conclude that the behavior we report here is due to other physics not yet explored by these models.

When a vortex moves through a stationary medium it experiences a Magnus force, which in superconductors is responsible for phenomena such as the Hall effect and quantum vortex nucleation [46,47]. At first glance, the Magnus force may appear to be a likely explanation for the observed vortex rotation. Therefore, before we relate the observed rotation of the VL to the noncentrosymmetric properties of the superconductor, we argue why the Magnus force cannot be responsible for this effect. Considering the VL under the application of a changing field, it is evident that the trajectory of vortices must, on average, follow a radial path as the density of vortices throughout the sample is changed. Therefore, the direction of the Magnus force acting on a vortex is opposite to that on a corresponding vortex on the other side of the sample, leading to a net torque. However, we discount the Magnus force as an explanation for several reasons. First, it is often negated by the spectral flow, leading to a vanishingly small effective Magnus force [47]. Further, we expect the Magnus force to be independent of field orientation, and the rocking curve width in Fig. 4(a) showed no systematic change with η, indicating a correspondingly direction-independent pinning, whereas the rotating behavior only appears when the field is close to the **a** axis. Finally, the Magnus force is linearly dependent on the carrier density, which varies with temperature in a superconductor, whereas no temperature dependence is observed in Fig. 2(a). This leads us to conclude that the Magnus force is not responsible for the rotation of the VL.

Both flux line pinning and a surface nucleation barrier to flux lines are known to lead to irreversibility of the VL. However, we do not consider these effects to be responsible for the rotation of the VL we observe. First, while our sample shows evidence of flux line pinning in the VL diffraction patterns and FWHM of the rocking curves, neither of these show unconventional behavior which might explain the rotation. The $|\mathbf{q}|$ of the VL diffraction spots in Fig. 2(e) lies between the expected values for a hexagonal and square lattice for both the FC and ZFC procedure, and is reversible throughout the rotation, indicating that barriers to flux flow and nucleation do not have a significant effect. The FWHM of the rocking curves in Fig. 4(a) also remains reasonably constant as a function of η, showing that the emergence of the rotating behavior is not related to a change in the effect of pinning or disorder, and indicating that a random distribution of pinning sites would be a reasonable assumption for this sample. It seems highly unlikely that a random distribution of pinning sites would have a coherent effect on the VL which is dependent on the direction of applied field. Furthermore, taking the sample through the cycle of the magnetic field which induces the rotation improves the lattice order slightly, as shown in Fig. 4(b), although since an identical ordering of the lattice takes place at values of η where the rotation does not this indicates that this process is not related to the rotation. Finally, we would expect a surface nucleation barrier in our geometry, a roughly cylindrical sample with the field applied nearly perpendicular to the long axis as shown in Fig. 1(e), to have an effect which is independent of the field orientation in the **ac** plane, and this is clearly not the case. We therefore discount pinning and surface nucleation effects as an origin of the rotation we observe.

Recently Ru_7B_3 was studied using μSR [48], and these measurements reveal the presence of spontaneous magnetic fields below the superconducting transition temperature which indicate that the superconducting state breaks time-reversal symmetry. In turn this gives rise to the problem of whether the time-reversal symmetry breaking (TRSB) superconducting state together with the broken inversion symmetry can drive the rotation of the VL. To address this possibility, we consider an extended Ginzburg-Landau (GL) approach by adding a magnetic contribution from the spontaneous magnetization:

$$F = F_s + F_m - \frac{\mathbf{B}^2}{8\pi} - \mathbf{B}\cdot\mathbf{M}. \quad (1)$$

Here, F_s is the superconducting part of the energy, which takes into account the uniaxial symmetry of the crystal and the absence of inversion symmetry for the C_{6v} point group in the presence of spin-orbit coupling. With $D = (-i\hbar\nabla - \frac{2e}{\hbar c}\mathbf{A})$, we write

$$F_s = \int \Big[\alpha|\psi|^2 + \frac{1}{2}\beta|\psi|^4 + \gamma|D\psi|^2 + \varepsilon\mathbf{n}\cdot\mathbf{B}\times(\psi^* D\psi + \psi D^*\psi^*)\Big] dV, \tag{2}$$

where α and β are phenomenological constants, γ is related to the average Fermi velocity, the term containing $\varepsilon\mathbf{n}\cdot\mathbf{B}\times\mathbf{j}$ is the so-called Lifshitz invariant arising from the loss of inversion symmetry, $\mathbf{n}$ is a vector parallel to the sixfold rotation axis $\mathbf{c}$, and ε is a parameter related to the strength of the spin-orbit coupling. We represent the possibility of spontaneous magnetic fields from TRSB by including a magnetic part of the free energy F_m, in a similar manner to a previous study focusing on the emergence of spontaneous magnetic fields at twin boundaries in NCS superconductors [49], which we define as

$$F_m = \int a|m|^2 + \frac{1}{2}b|m|^4 + d_{ij}\nabla m_i \nabla m_j \, dV, \tag{3}$$

where m is the density of the magnetic-moment component.

Following Abrikosov's procedure [50], which is written out in detail in the Appendix, we find an expression for the magnetization $\mathbf{M}$ of a superconductor below the upper critical field H_{c2},

$$\mathbf{M} = \frac{\langle(\mathbf{B}-\mathbf{H})\rangle}{4\pi} = \mathbf{m_0} + \frac{\langle\delta\mathbf{B}\rangle}{4\pi}, \tag{4}$$

and an expression for the current in the form

$$\mathbf{j} = \frac{1}{4\pi}\mathbf{rot}(\delta\mathbf{B} - 4\pi\mathbf{m_1} - 8\pi\varepsilon\mathbf{n}|\psi_0|^2) = \gamma\left[\psi_0^*\left(-i\hbar\nabla - \frac{2e}{\hbar c}\mathbf{A_0}\right)\psi_0 + \psi_0\left(i\hbar\nabla - \frac{2e}{\hbar c}\mathbf{A_0}\right)\psi_0^*\right]. \tag{5}$$

In these expressions, $\mathbf{m}_0$ is the spontaneous magnetization and $\delta\mathbf{B}$ and $\mathbf{m}_1$ are corrections to the magnetic field and magnetization due to the presence of the flux lattice. The brackets $\langle\ldots\rangle$ define the spatial average to be calculated over the unit cell of the vortex lattice. After some algebra, detailed in the Appendix, we arrive at the expression

$$\frac{M-m_0}{H-H_{c2}} = \frac{\left(a+3bm_0^2\right)\left(\frac{2\pi}{\Phi_0}\gamma+2\varepsilon\right)^2}{2\beta\left(a+3bm_0^2-2\pi\right)+4\pi\left(\frac{2\pi}{\Phi_0}\gamma+2\varepsilon\right)^2\left(a+3bm_0^2\right)}\frac{\langle|\psi_0|^2\rangle^2}{\langle|\psi_0|^4\rangle}, \tag{6}$$

where m_0 is the density of the magnetic moment of the spontaneous magnetization. The right side in Eq. (6) is inversely proportional to the Abrikosov parameter, β_A. The minimal value of β_A corresponds to a global minimum of the GL free energy for a superconductor and determines the energetically favorable VL configuration. For a conventional single-band superconductor the Abrikosov parameter is material independent and predicts a hexagonal lattice with a degenerate orientation with respect to the crystal. In our case, however, we can see from Eq. (6) that for a noncentrosymmetric superconductor with TRSB this universality of β_A is lost, and the configuration of the lattice starts to depend on the external magnetic field, microscopic magnetization, and the superconducting properties of the system. We therefore introduce an altered Abrikosov parameter, β_A':

$$\beta_A' \sim \frac{2\beta\left(a+3bm_0^2-2\pi\right)+4\pi\left(\frac{2\pi}{\Phi_0}\gamma+2\varepsilon\right)^2\left(a+3bm_0^2\right)}{\left(a+3bm_0^2\right)\left(\frac{2\pi}{\Phi_0}\gamma+2\varepsilon\right)^2}\frac{\langle|\psi_0|^4\rangle}{\langle|\psi_0|^2\rangle^2}. \tag{7}$$

Therefore, from the determination of the value and behavior of the spontaneous magnetization m_0 and knowing the exact values of phenomenological parameters for the given superconducting compound, we can calculate β_A' and then the corresponding free energy. However, at this point these parameters and their behavior as a function of applied field and field history are not known. To illustrate the coupling of the VL to the orientation of the crystal lattice, we performed calculations of the free energy as a function of the angle ϕ between the basis vectors of the VL and the crystal axes, assuming an arbitrary value of m_0. The orientation of the VL, ϕ, appears from the averaging procedure for the order parameter within the unit cell of the lattice [26,51]. Critically, the appearance of vector components in Eq. (4), where a spatial average is carried out over the unit cell of the VL, and Eq. (5), which results in a different form for supercurrents along different crystal axes, leads to an orientation dependence of the free energy. Using a trial set of numerical parameters: $a = -1.95$, $b = 0.83$, $\beta = 1.5$, $\gamma = 3.2$, and $\varepsilon = 1.3$, we plot the free energy as a function of ϕ in Fig. 5. The free energy minimum shifts with changing field, showing that the coupling of the VL to the broken inversion symmetry and spontaneous magnetization of TRSB gives the VL a field-dependent orientation. While these parameters are related to microscopic properties of the system, not all of them are currently known, and so the above were chosen purely to illustrate the rotation of the VL which we observed. We assume that the spontaneous moments are undergoing hysteresis, leading to a hysteresis in the orientation, but in order to correctly model this it will be necessary to know explicit values of these parameters, the spontaneous magnetization, and how these interact with the more complex vortex structures of NCS superconductors. We do not yet know these, so we leave the theory as an illustration of the driving force of the rotation.

Our model demonstrates that both the spontaneous fields present under TRSB and the effect of broken inversion symmetry inseparably couple to the orientation and structure of the VL. Since the rotation of the VL is only observed when

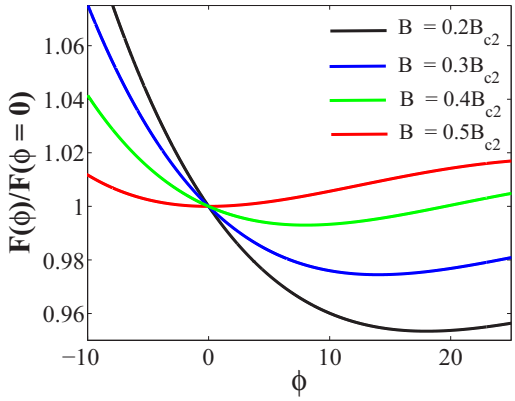

FIG. 5. Free energy of VL vs the rotation angle as a function of magnetic field, for the GL model described in the text.

the field is close to the **ab** plane, and the Lifshitz invariant, which is proportional to $\mathbf{n} \cdot \mathbf{B} \times \mathbf{j}$, drops out of the free energy when the applied magnetic field is parallel to the **c** axis, the model suggests that the effect of broken inversion symmetry is necessary for the rotation to appear. The model also predicts that the spontaneous moments which arise from TRSB are also coupled to the VL orientation. These should be randomly oriented in zero field, and the hysteresis in the VL orientation suggests that they are aligned by the applied magnetic field and undergo a hysteresis of their own, driving the changes is the VL orientation. The alignment and hysteresis of TRSB fields by an external applied field has already been observed in the heavy-fermion superconductor UPt_3 [52], and while the TRSB fields are very small, on the order of 1 G, we note first that the orientation and coordination of the VL are notoriously sensitive to small changes in its free energy [53], and second that superconducting states which break time-reversal symmetry tensorially couple the supercurrent to gradients in the order parameter, resulting in additional field components within the mixed state [2]. This is similar to the appearance of tangential fields within the vortex lattice of NCS superconductors, although its effects have not been studied and it may mean that the TRSB fields are not limited to those observed in zero field by techniques such as μSR. Furthermore, it has also been found that superconducting order parameters which break time-reversal symmetry can have a significant effect on the VL through other mechanisms, forming vortex cores which break rotational symmetry and result in frustrated lattices [54], and so we therefore consider the effect of TRSB to be relevant despite the small size of the spontaneous field it produces.

The GL approach we use here should be considered a qualitative model, to illustrate the coupling of NCS superconductivity and TRSB to the behavior of the VL. GL theory is valid close to H_{c2}, and while we do see the VL rotation near the upper critical field this also persists to much lower fields where the theory may not be quantitatively accurate. At present, the model not only demonstrates the presence of the rotation, but it also captures its anisotropic nature; that is to say, it only occurs in one direction. Furthermore, the presence of a shifting minimum in the free energy as a function of ϕ illustrates why the rotated states appear so stable to both perturbations in field and thermal fluctuations, as they are new equilibrium states as opposed to metastable states. However, before the model can truly capture this behavior, it requires several improvements. Most notably, other contributions to $F(\phi)$, such as Fermi velocity anisotropy and gap anisotropy, must be included, as while the Abrikosov parameter predicts a degenerate orientation for a conventional superconductor [50], this is never observed and the VL always chooses a specific orientation due to these physics which are not captured by the original model. It is not yet known what effect the broken inversion symmetry will have on the results of theories developed after Abrikosov's, which have been used to explain the VL orientation and coordination in centrosymmetric systems, which were discussed earlier, if any. Our phenomenological approach also did not take into account the possible presence of a small triplet component of the order parameter, as Ru_7B_3 has been suggested to be a pure *s*-wave system from magnetization measurements [38], although the data were not taken down to a low enough fraction of T/T_c to be certain. In this case the expression for the Abrikosov parameter will be more complex, allowing for substantially richer behavior of the VL. In order to develop a more complete understanding of the VL behavior in this system, it will be necessary to perform microscopic calculations which include details of the anisotropy in the Fermi velocity and the superconducting gap as well as the ASOC and TRSB. Furthermore, it is imperative to investigate other NCS and TRSB superconductors under these conditions to further elucidate the contributions of TRSB and broken inversion symmetry to the VL behavior we observe here.

V. CONCLUSIONS

We have performed SANS measurements on the VL of the noncentrosymmetric superconductor Ru_7B_3, finding a VL orientation which is strongly dependent on the field history of the sample within the superconducting state. This is unprecedented behavior, which has not been predicted by previous theories of the VL. To address this, we construct a model of the VL from the phenomenological GL theory which includes the Lifshitz invariant suitable for our material and the magnetic contribution of the spontaneous magnetization due to TRSB phenomena. We find that the Abrikosov parameter, a geometric object which relates to the orientation and coordination of the VL, gains a complex prefactor in the case of a noncentrosymmetric superconductor with TRSB, which couples the parameter to the spontaneous magnetization and superconducting properties of the system. We therefore predict that the spontaneous magnetization has hysteretic behavior in Ru_7B_3, which in turn results in a corresponding hysteresis in the VL orientation.

ACKNOWLEDGMENTS

This project was funded by the German Research Foundation (DFG) through the research grants IN 209/3-2, IN 209/6-1, and the Research Training Group GRK 1621. A.S.S. acknowledges support from the International Max Planck Research School for Chemistry and Physics of Quantum Materials (IMPRS-CPQM). The work at Warwick was supported by EPSRC, UK, through Grant No. EP/M028771/1.

APPENDIX

Our approach is based on a Ginzburg-Landau (GL) functional

$$F = F_s + F_m - \frac{\mathbf{B}^2}{8\pi} - \mathbf{B}\cdot\mathbf{M}, \tag{A1}$$

with the terms as defined previously and the Lifshitz invariant which describes the ASOC given in Eq. (2). It is important to note that the contribution to the GL energy of the Lifshitz invariant gives rise to different phenomena in noncentrosymmetric superconductors, in particular FFLO-like phases, magnetoelectric effects, and exotic vortex states.

We also introduce a magnetic part of the free energy from the spontaneous magnetization due to TRSB, which is defined as

$$F_m = \int a|m|^2 + \frac{1}{2}b|m|^4 + d_{ij}\nabla m_i \nabla m_j \, dV, \tag{A2}$$

where m is the density of the magnetic-moment component. By minimizing the GL free energy with respect to the order parameter and the vector potential the following GL equations are found:

$$\alpha|\psi| + \beta|\psi|^3 + \gamma\left(-i\hbar\nabla - \frac{2e}{\hbar c}\mathbf{A}\right)^2\psi + \varepsilon\mathbf{n}\cdot\mathbf{B}\times\left(-i\hbar\nabla - \frac{2e}{\hbar c}\mathbf{A}\right)\psi = 0 \tag{A3}$$

and

$$\mathbf{j} = \frac{2ie}{\hbar c}\gamma\left[\psi^*\left(-i\hbar\nabla - \frac{2e}{\hbar c}\mathbf{A}\right)\psi + \psi\left(i\hbar\nabla - \frac{2e}{\hbar c}\mathbf{A}\right)\psi^*\right] + \frac{4e}{\hbar c}\varepsilon|\psi|^2\mathbf{B}. \tag{A4}$$

For simplicity we choose the gauge $\mathbf{A} = Bx(0, 1, 0)$. Near the upper critical field we can linearize the GL Eq. (A3):

$$\alpha\psi - \gamma\left[\frac{\partial^2}{\partial x^2} + \left(\frac{\partial^2}{\partial y^2} - \frac{2ieB_{c2}x}{\hbar c}\right)^2\right]\psi + \varepsilon B_{c2}\left[\frac{\partial}{\partial x} + \left(\frac{\partial}{\partial y} - \frac{2ieB_{c2}x}{\hbar c}\right)\right]\psi = 0. \tag{A5}$$

The lowest eigenvalue of the GL operator corresponds to the order parameter:

$$\psi(x, y) = \sum_{n=-\infty}^{\infty} C_n \exp(ikny) \times \exp\left[-\frac{\pi B_{c2}}{\Phi_0}\left(x - \frac{kn\Phi_0}{2\pi B_{c2}} - \frac{\Phi_0}{2\pi}\frac{\varepsilon}{\gamma}\right)^2\right]. \tag{A6}$$

Equation (A6) for the vortex lattice solution coincides with that of Abrikosov for a single-band superconductor, but due to the presence of the Lifshitz invariant it obtains the so-called helical phase factor $\frac{\Phi_0}{2\pi}\frac{\varepsilon}{\gamma}$, which can lead to the enhancement of the upper critical field. At a magnetic field B slightly below B_{c2} the mixed state appears and the order parameter amplitude, the magnetic moment, and the vector potential acquire the small correction

$$\psi = \psi_0 + \psi_1, \ \mathbf{m} = \mathbf{m_0} + \mathbf{m_1}, \ \mathbf{A} = \mathbf{A_0} + \mathbf{A_1}, \tag{A7}$$

where $\mathbf{A_1} = (0, (H - 4\pi m_0 - B_{c2})x, 0) + \delta\mathbf{A}$, $\mathbf{m}_0$ is the spontaneous magnetization, $\mathbf{A_0} = Bx(0, 1, 0)$, and $\mathbf{m}_1$ and ψ_1 are the corrections due to the presence of the mixed state to the magnetization and order parameter, respectively. The corresponding magnetic induction is

$$\mathbf{B} = \mathbf{H} + 4\pi\mathbf{m_0} + \delta\mathbf{B}. \tag{A8}$$

The full magnetization of the system is

$$\mathbf{M} = \frac{\langle(\mathbf{B} - \mathbf{H})\rangle}{4\pi} = \mathbf{m_0} + \frac{\langle\delta\mathbf{B}\rangle}{4\pi}, \tag{A9}$$

where brackets $\langle\ldots\rangle$ define the spatial average. Taking into account Eq. (A4) one can get an expression for the current in the form

$$\mathbf{j} = \frac{1}{4\pi}\mathbf{rot}\left(\delta\mathbf{B} - 4\pi\mathbf{m_1} - 8\pi\varepsilon\mathbf{n}|\psi_0|^2\right) = \gamma\left[\psi_0^*\left(-i\hbar\nabla - \frac{2e}{\hbar c}\mathbf{A_0}\right)\psi_0 + \psi_0\left(i\hbar\nabla - \frac{2e}{\hbar c}\mathbf{A_0}\right)\psi_0^*\right]. \tag{A10}$$

Representing Eq. (A10) through the x and y scalar components and taking into account the relation $\frac{\partial\psi_0}{\partial x} = (-i\frac{\partial}{\partial y} - \frac{2ieB_{c2}}{\hbar c})\psi_0$, one can rewrite

$$\frac{\partial}{\partial x}(\delta B - 4\pi m_1 - 8\pi\varepsilon|\psi_0|^2) = 4\pi\frac{2\pi}{\Phi_0}\gamma\frac{\partial|\psi_0|^2}{\partial x} \tag{A11}$$

and

$$\frac{\partial}{\partial y}(\delta B - 4\pi m_1 - 8\pi\varepsilon|\psi_0|^2) = 4\pi\frac{2\pi}{\Phi_0}\gamma\frac{\partial|\psi_0|^2}{\partial y}. \tag{A12}$$

This gives the expression for the correction δB:

$$\delta B = 4\pi\frac{2\pi}{\Phi_0}\gamma|\psi_0|^2 + 4\pi m_1 + 8\pi\varepsilon|\psi_0|^2. \tag{A13}$$

To find m_1 we consider the variation of the free energy given by Eq. (A2) with respect to m:

$$2am + 2bm^3 + 2d_{ij}\nabla^2 m - B = 0; \tag{A14}$$

hence the correction m_1 for the magnetization is determined by the equation

$$\left(2a + 6bm_0^2 + 2d_{ij}\nabla^2\right)m_1 - \delta B = 0. \tag{A15}$$

If we assume that the magnetic coherence length is smaller than the size of the vortex core then one can neglect the Laplacian term in Eq. (A15), and taking into account Eq. (A13) we get the expression for

$$m_1 = \frac{\frac{(2\pi)^2}{\Phi_0}\gamma|\psi_0|^2 + 4\pi\varepsilon|\psi_0|^2}{a + 3bm_0^2 - 2\pi}. \tag{A16}$$

According to Eq. (A9) below transition to the superconducting state the magnetization follows

$$M - m_0 = \left\langle \frac{2\pi}{\Phi_0}\gamma|\psi_0|^2 + m_1 + 2\varepsilon|\psi_0|^2 \right\rangle. \tag{A17}$$

Now we proceed to find an average of Eq. (A17). Based on the linearized form of the GL Eq. (A5), after long but straightforward calculations we obtain

$$\langle \mathbf{j}\cdot\mathbf{A_1} + 2\beta|\psi_0|^4\rangle = 0. \tag{A18}$$

Using Eqs. (A11) and (A13) for the current and small correction of δB, respectively, we have

$$\left\langle \left(\frac{2\pi}{\Phi_0}\gamma|\psi_0|^2 - 2\varepsilon|\psi_0|^2\right)(H - H_{c2}) + \left(\frac{2\pi}{\Phi_0}\gamma|\psi_0|^2 - 2\varepsilon|\psi_0|^2\right)\delta B + 2\beta|\psi_0|^4 \right\rangle = 0. \tag{A19}$$

Thus below the upper critical field the magnetization decrease is

$$\left\langle \left(\frac{2\pi}{\Phi_0}\gamma|\psi_0|^2 - 2\varepsilon|\psi_0|^2\right)(H - H_{c2}) + \left(\frac{2\pi}{\Phi_0}\gamma|\psi_0|^2 - 2\varepsilon|\psi_0|^2\right)\delta B + 2\beta|\psi_0|^4 \right\rangle = 0, \tag{A20}$$

and the final expression for Eq. (A20) takes the form

$$M - m_0 = \frac{\left(a + 3bm_0^2\right)\left(\frac{2\pi}{\Phi_0}\gamma + 2\varepsilon\right)^2}{2\beta\left(a + 3bm_0^2 - 2\pi\right) + 4\pi\left(\frac{2\pi}{\Phi_0}\gamma + 2\varepsilon\right)^2\left(a + 3bm_0^2\right)} \frac{\langle|\psi_0|^2\rangle^2}{\langle|\psi_0|^4\rangle}\left(H - H_{c2}\right). \tag{A21}$$

The prefactor before the expression $(H - H_{c2})$ can be interpreted as the relation, known for a single-band superconductor, $1/4\pi\beta_A(2k^2 - 1)$, where k is the GL parameter and β_A is the Abrikosov parameter. In the case of a noncentrosymmetric superconductor with TRSB the universality of this expression is lost through the introduction of the prefactor in Eq. (A21). The presence of vector components in the preceding spatial average calculations couples the VL orientation to the crystal lattice through the TRSB moments and the ASOC. Based on Eq. (A6) for the order parameter we can obtain the value of β_A', the modified Abrikosov parameter including the prefactor from Eq. (A21). Taking this into account, the free energy of a superconductor given by Eq. (A1) can be reduced to the form

$$F = F_m + \frac{B^2}{8\pi} - \frac{(B - B_{c2})^2}{1 + \beta_A'(2k^2 - 1)}. \tag{A22}$$

[1] E. Bauer, G. Hilscher, H. Michor, C. Paul, E. W. Scheidt, A. Gribanov, Y. Seropegin, H. Noël, M. Sigrist, and P. Rogl, Phys. Rev. Lett. **92**, 027003 (2004).

[2] M. Sigrist and K. Ueda, Rev. Mod. Phys. **63**, 239 (1991).

[3] L. P. Gor'kov and E. I. Rashba, Phys. Rev. Lett. **87**, 037004 (2001).

[4] P. A. Frigeri, D. F. Agterberg, A. Koga, and M. Sigrist, Phys. Rev. Lett. **92**, 097001 (2004).

[5] M. Sigrist, D. Agterberg, P. Frigeri, N. Hayashi, R. Kaur, A. Koga, I. Milat, K. Wakabayashi, and Y. Yanase, J. Magn. Magn. Mater. **310**, 536 (2007).

[6] H. Q. Yuan, D. F. Agterberg, N. Hayashi, P. Badica, D. Vandervelde, K. Togano, M. Sigrist, and M. B. Salamon, Phys. Rev. Lett. **97**, 017006 (2006).

[7] R. P. Kaur, D. F. Agterberg, and M. Sigrist, Phys. Rev. Lett. **94**, 137002 (2005).

[8] Y. Nagai, Y. Kato, and N. Hayashi, J. Phys. Soc. Jpn. **75**, 043706 (2006).

[9] N. Hayashi, Y. Kato, P. Frigeri, K. Wakabayashi, and M. Sigrist, Physica C **437-438**, 96 (2006).

[10] P. A. Frigeri, D. F. Agterberg, I. Milat, and M. Sigrist, Eur. Phys. J. B **54**, 435 (2006).

[11] M. Laver and E. M. Forgan, Nat. Commun. **1**, 45 (2010).

[12] K. M. Suzuki, K. Inoue, P. Miranović, M. Ichioka, and K. Machida, J. Phys. Soc. Jpn. **79**, 013702 (2010).

[13] R. Gilardi, J. Mesot, A. Drew, U. Divakar, S. L. Lee, E. M. Forgan, O. Zaharko, K. Conder, V. K. Aswal, C. D. Dewhurst, R. Cubitt, N. Momono, and M. Oda, Phys. Rev. Lett. **88**, 217003 (2002).

[14] J. S. White, V. Hinkov, R. W. Heslop, R. J. Lycett, E. M. Forgan, C. Bowell, S. Strässle, A. B. Abrahamsen, M. Laver, C. D. Dewhurst, J. Kohlbrecher, J. L. Gavilano, J. Mesot, B. Keimer, and A. Erb, Phys. Rev. Lett. **102**, 097001 (2009).

[15] J. S. White, C. J. Bowell, A. S. Cameron, R. W. Heslop, J. Mesot, J. L. Gavilano, S. Strässle, L. Mächler, R. Khasanov, C. D. Dewhurst, J. Karpinski, and E. M. Forgan, Phys. Rev. B **89**, 024501 (2014).

[16] A. S. Cameron, J. S. White, A. T. Holmes, E. Blackburn, E. M. Forgan, R. Riyat, T. Loew, C. D. Dewhurst, and A. Erb, Phys. Rev. B **90**, 054502 (2014).

[17] H. Kawano-Furukawa, C. J. Bowell, J. S. White, R. W. Heslop, A. S. Cameron, E. M. Forgan, K. Kihou, C. H. Lee, A. Iyo, H. Eisaki, T. Saito, H. Fukazawa, Y. Kohori, R. Cubitt, C. D. Dewhurst, J. L. Gavilano, and M. Zolliker, Phys. Rev. B **84**, 024507 (2011).

[18] R. Morisaki-Ishii, H. Kawano-Furukawa, A. S. Cameron, L. Lemberger, E. Blackburn, A. T. Holmes, E. M. Forgan, L. M. DeBeer-Schmitt, K. Littrell, M. Nakajima, K. Kihou, C. H. Lee, A. Iyo, H. Eisaki, S. Uchida, J. S. White, C. D. Dewhurst, J. L. Gavilano, and M. Zolliker, Phys. Rev. B **90**, 125116 (2014).

[19] M. R. Eskildsen, P. L. Gammel, B. P. Barber, U. Yaron, A. P. Ramirez, D. A. Huse, D. J. Bishop, C. Bolle, C. M. Lieber, S. Oxx, S. Sridhar, N. H. Andersen, K. Mortensen, and P. C. Canfield, Phys. Rev. Lett. **78**, 1968 (1997).
[20] M. Ichioka, A. Hasegawa, and K. Machida, Phys. Rev. B **59**, 8902 (1999).
[21] V. G. Kogan, M. Bullock, B. Harmon, P. Miranović, L. Dobrosavljević-Grujić, P. L. Gammel, and D. J. Bishop, Phys. Rev. B **55**, R8693(R) (1997).
[22] V. G. Kogan, P. Miranović, L. Dobrosavljević-Grujić, W. E. Pickett, and D. K. Christen, Phys. Rev. Lett. **79**, 741 (1997).
[23] M. Franz, I. Affleck, and M. H. S. Amin, Phys. Rev. Lett. **79**, 1555 (1997).
[24] N. Nakai, P. Miranović, M. Ichioka, and K. Machida, Phys. Rev. Lett. **89**, 237004 (2002).
[25] P. Das, C. Rastovski, T. R. O'Brien, K. J. Schlesinger, C. D. Dewhurst, L. DeBeer-Schmitt, N. D. Zhigadlo, J. Karpinski, and M. R. Eskildsen, Phys. Rev. Lett. **108**, 167001 (2012).
[26] T. Hirano, K. Takamori, M. Ichioka, and K. Machida, J. Phys. Soc. Jpn. **82**, 063708 (2013).
[27] S. Yip, J. Low Temp. Phys. **140**, 67 (2005).
[28] M. K. Kashyap and D. F. Agterberg, Phys. Rev. B **88**, 104515 (2013).
[29] Y. Matsunaga, N. Hiasa, and R. Ikeda, Phys. Rev. B **78**, 220508 (2008).
[30] N. Hiasa, T. Saiki, and R. Ikeda, Phys. Rev. B **80**, 014501 (2009).
[31] M. Oka, M. Ichioka, and K. Machida, Phys. Rev. B **73**, 214509 (2006).
[32] C.-K. Lu and S. Yip, Phys. Rev. B **77**, 054515 (2008).
[33] C.-K. Lu and S. Yip, J. Low Temp. Phys. **155**, 160 (2009).
[34] L. Lemberger, Vortex lattice in conventional and unconventional superconductors, Ph.D. thesis, University of Birmingham, 2016.
[35] B. Aronsson, Acta Chem. Scand. **13**, 109 (1959).
[36] R. Singh, N. Parzyk, M. Lees, D. Paul, and G. Balakrishnan, J. Cryst. Growth **395**, 22 (2014).
[37] B. Matthias, V. Compton, and E. Corenzwit, J. Phys. Chem. Solids **19**, 130 (1961).
[38] L. Fang, H. Yang, X. Zhu, G. Mu, Z.-S. Wang, L. Shan, C. Ren, and H.-H. Wen, Phys. Rev. B **79**, 144509 (2009).
[39] N. Kase and J. Akimitsu, J. Phys. Soc. Jpn. **78**, 044710 (2009).
[40] C. D. Dewhurst, Meas. Sci. Technol. **19**, 034007 (2008).
[41] Experiment carried out under doi:10.5291/ILL-DATA.5-42-397.
[42] Experiment carried out under doi:10.5291/ILL-DATA.5-42-416.
[43] A. Heinemann and S. Mühlbauer, J. large-scale Res. Fac. **1**, A10 (2015).
[44] A. T. Holmes, Phys. Rev. B **90**, 024514 (2014).
[45] A. Pautrat, M. Aburas, C. Simon, P. Mathieu, A. Brûlet, C. D. Dewhurst, S. Bhattacharya, and M. J. Higgins, Phys. Rev. B **79**, 184511 (2009).
[46] G. Blatter, M. V. Feigel'man, V. B. Geshkenbein, A. I. Larkin, and V. M. Vinokur, Rev. Mod. Phys. **66**, 1125 (1994).
[47] E. B. Sonin, Phys. Rev. B **55**, 485 (1997).
[48] N. A. Parzyk, Muon and neutron studies of unconventional superconductors, Ph.D. thesis, Univerisy of Warwick, 2014.
[49] M. Achermann, T. Neupert, E. Arahata, and M. Sigrist, J. Phys. Soc. Jpn. **83**, 044712 (2014).
[50] A. A. Abrikosov, Zh. Eksp. Teor. Fiz. **32**, 1442 (1957) [Sov. Phys. JETP **5**, 1174 (1957)].
[51] D. Saint-James, E. Thomas, and G. Sarma, *Type II Superconductivity* (Pergamon Press, 1969).
[52] E. R. Schemm, W. J. Gannon, C. M. Wishne, W. P. Halperin, and A. Kapitulnik, Science **345**, 190 (2014).
[53] W. H. Kleiner, L. M. Roth, and S. H. Autler, Phys. Rev. **133**, A1226 (1964).
[54] T. A. Tokuyasu, D. W. Hess, and J. A. Sauls, Phys. Rev. B **41**, 8891 (1990).